ACS APPLIED MATERIALS & INTERFACES

Research Article

www.acsami.org

Fine Tuning of Fluorene-Based Dye Structures for High-Efficiency *p*-Type Dye-Sensitized Solar Cells

Zonghao Liu,[†] Wenhui Li,[†] Sanjida Topa,[‡] Xiaobao Xu,[†] Xianwei Zeng,[†] Zhixin Zhao,*[,†] Mingkui Wang,*[,†] Wei Chen,[†] Feng Wang,[‡] Yi-Bing Cheng,[†,§] and Hongshan He*[,∥]

[†]Michael Grätzel Center for Mesoscopic Solar Cells, Wuhan National Laboratory for Optoelectronics, School of Optical and Electronic Information, Huazhong University of Science and Technology, Wuhan 430074, People's Republic of China

[∥]Department of Chemistry, Eastern Illinois University, Charleston, Illinois 61920, United States

[§]Department of Materials Engineering, Monash University, Melbourne, Victoria 3800, Australia

[‡]Molecular Model Discovery Laboratory, Department of Chemistry & Biotechnology, Faculty of Science, Engineering and Technology, Swinburne University of Technology, PO Box 218, Hawthorn, Victoria 3122, Australia

Supporting Information

ABSTRACT: We report on an experimental study of three organic push−pull dyes (coded as zzx-op1, zzx-op1−2, and zzx-op1−3) featuring one, two, and three fluorene units as spacers between donors and acceptors for *p*-type dye-sensitized solar cells (*p*-DSSC). The results show increasing the number of spacer units leads to obvious increases of the absorption intensity between 300 nm and 420 nm, a subtle increase in hole driving force, and almost the same hole injection rate from dyes to NiO nanoparticles. Under optimized conditions, the zzx-op1−2 dye with two fluorene spacer units outperforms other two dyes in *p*-DSSC. It exhibits an unprecedented photocurrent density of 7.57 mA cm^{-2} under full sun illumination (simulated AM 1.5G light illumination, 100 mW cm^{-2}) when the I^-/I_3^- redox couple and commercial NiO nanoparticles were used as an electrolyte and a semiconductor, respectively. The cells exhibited excellent long-term stability. Theoretical calculations, impedance spectroscopy, and transient photovoltage decay measurements reveal that the zzx-op1−2 exhibits lower photocurrent losses, longer hole lifetime, and higher photogenerated hole density than zzx-op1 and zzx-op1−3. A dye packing model was proposed to reveal the impact of dye aggregation on the overall photovoltaic performance. Our results suggest that the structural engineering of organic dyes is important to enhance the photovoltaic performance of *p*-DSSC.

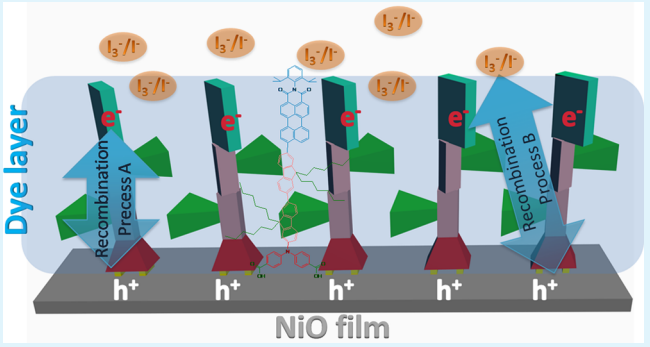

KEYWORDS: *p-type dye-sensitized solar cells, organic sensitizer, fluorene, charge recombination, NiO*

INTRODUCTION

It is still challenging to convert solar energy to electricity in a cost-effective manner. Among many devices, dye-sensitized solar cells, especially *n*-type dye-sensitized solar cells (*n*-DSSC), have been extensively investigated.[1−3] Recently, *p*-type dye-sensitized solar cells (*p*-DSSC) become attractive because of their potential to construct high-efficiency tandem cells with *n*-DSSC through molecular engineering of light-harvesting materials.[4−8] However, low photocurrent densities from state-of-the-art *p*-DSSC limit output of current density of tandem cells; therefore, it has become a bottleneck for the development of high-efficiency tandem cells.[4−7] To date, the highest photocurrent density for *p*-DSSC is 7.0 mA cm^{-2},[9] which is much lower than the current density of its counterpart, which has a range of 15−20 mA cm^{-2}.[2,3,10−13] The highest power conversion efficiency (PCE) of *p*-DSSC is 1.30%,[14] which is also far below the record PCE of 13.0% in *n*-DSSC.[10,13]

A key challenge in *p*-DSSC is how to reduce the charge recombination between the injected hole in the semiconductor and the reduced dyes or electrolytes.[4,5,15−18] One strategy is to use rationally designed light-harvesting material to retard those processes. One method is to engineer push−pull dyes to enhance the hole injection capability.[17,19−27] Sun et al. synthesized triphenylamine-based push−pull dyes and found that the photocurrent density increased significantly, to 5.48 mA cm^{-2}, on NiO films,[19,28] which was much higher than its counterparts (coumarin dye, C343) without such a structure. Bäuerle et al. designed an oligothiophene-functionalized push−pull dye, coded as PMI-6T-TPA, and a photocurrent density of 5.35 mA cm^{-2} was obtained in similar cells.[7] Recently, Bach et al. reported a record photocurrent density of 7.0 mA cm^{-2}

Received: April 15, 2014
Accepted: June 11, 2014
Published: June 11, 2014

when the same PMI-6T-TPA dye and the nanostructured NiO microballs were used.[9] Previously, we designed three fluorene-based dyes—zzx-op1, zzx-op2, and zzx-op3—to modulate hole injection in *p*-DSSC.[29] Our study showed that ~0.80 eV of hole injection driving force was needed to achieve a high hole injection quantum yield when NiO and I^-/I_3^- were used in the devices. The dye zzx-op1 with a di(*p*-carboxy)phenylamine (DCPA) as a donor, a perylenemonoimide (PMID) as an electron acceptor, and one fluorene (FLU) as a spacer produced a photocurrent density of 4.38 mA cm^{-2} with a PCE of 0.184%, indicating the promising of this dye for *p*-DSSC. However, fast charge recombination between the injected hole and the reduced dye was observed in zzx-op1-sensitized *p*-DSSC. This comes primarily from a short distance between the PMID donor the surface of NiO nanoparticles, which results in a significant photocurrent losses.[5,7]

Two new oligo-fluorene-based dyes, zzx-op1−2 and zzx-op1−3, were designed to address this issue (Scheme 1). In these dyes, the DCPA was used as a donor, a PMID as an electron acceptor, two and three conjugated 9,9-dihexyl-9H-fluorene (FLU) units were used as spacers. We expect this design will tune the dye structure to retard the aforementioned recombinations. It was found that the insertion of FLU units only changed the hole driving force subtly. However, the FLU units extended the distance between PMID and the surface of NiO nanoparticles and retarded the charge recombination between the injected hole and the reduced dye, which reduced the photocurrent losses effectively.[7] As a result, dyes zzx-op1−2 and zzx-op1−3 showed much better performance than zzx-op1. Under optimized conditions, an unprecedented photocurrent density of 7.56 mA cm^{-2} was obtained.

Scheme 1. Structure of Dyes zzx-op1, zzx-op1−2, and zzx-op1−3

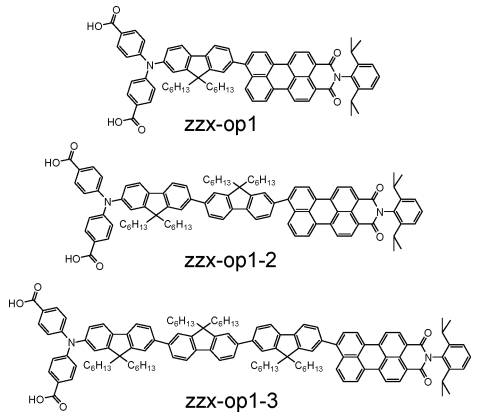

RESULTS AND DISCUSSION

The synthesis of dyes zzx-op1−2 and zzx-op1−3 is shown in Scheme 2. Brominated oligo-fluorene compounds **1** and **6** were synthesized according to the literature procedures,[30,31] and reacted with diphenylamine under Buchwald−Hartwig reaction conditions to give diphenylamine−oligofluorene derivatives **3** and **7** in yields of 23% and 25%, respectively.[22] Both then reacted with the borate−perylenemonoimide derivative (**4**) under Pd-catalyzed Suzuki cross-coupling reaction conditions to produce compounds **5** and **8** in yields of 88% and 83%, respectively.[22] They were then hydrolyzed in the presence of TFA to give zzx-op1−2 and zzx-op1−3 in yields of 89% and 82%, respectively.[22] The structures and purity of all intermediates and final compounds were characterized by NMR and high-resolution mass spectrometry (see details in the Electronic Supporting Information (ESI)).

The ultraviolet−visible (UV-vis) absorption spectra of all three dyes in THF are quite similar to each other. The details have been tabulated in Table 1. As shown in Figure 1, two major absorption bands in the range of 300−600 nm were observed for three dyes. The first band (~360 nm) comes from the FLU linker and the donor group. When the spectra were normalized at 520 nm, the intensity of the first band increased with the number of FLU repeating units. The second band (~520 nm) presented a small blue-shifted due to the $\pi-\pi^*$ electron transition. This result is likely attributed to the aggregation of dyes in THF. When these dyes were stained on the NiO films, the absorption spectra became broader compared to those in solution (see Figure S1 in the ESI), and peak positions shifted to a shorter wavelength region. The broadened spectra may be ascribed to the aggregation on the surface of semiconductor, and the shifted peak positions may be ascribed to the deprotonation of the carboxylic acid or the different polarity of the medium and H-aggregation.[25,32] The fluorescence spectra (see Figure S2 in the ESI) of three dyes were also quite similar to each other. The zero−zero transition energy (E_{0-0}(S*)), determined from the crossing points of the normalized UV-vis absorption spectra and the fluorescence spectra of the dyes in THF (see Figure S2 in the ESI), were 2.21 eV for zzx-op1, 2.23 eV for zzx-op1−2, and 2.23 eV for zzx-op1−3, respectively. This indicated that increasing the number of FLU repeating units did not change the energy gap of the dyes significantly. The E_{ox} and E_{red}, obtained from cyclic voltammograms (see Figure S3 in the ESI) for three dyes were almost identical to each other. As a result, the hole injection driving forces (ΔG_{inj} for three dyes were evaluated to be −0.82 eV for zzx-op1, −0.82 eV for zzx-op1−2, and −0.83 eV for zzx-op1−3, respectively. Similar results for dye regeneration driving force were also observed (−0.66 eV for zzx-op1, −0.68 eV for zzx-op1−2, and −0.67 eV for zzx-op1−3, respectively). Those results indicate that the three dyes are energetically favorable for the operation of *p*-DSSC.

The photocurrent−voltage curves of the champion *p*-DSSC with the three dyes in different solvents are shown in Figure 2, and the averaged devices performance is shown in the ESI. The devices photovoltaic parameters are listed in Table 2. Acetonitrile has been widely used as a solvent for preparation of dye solution; however, we found that the three dyes exhibited low solubility in acetonitrile and the resulting NiO films were poorly stained. To overcome this problem, acetonitrile/THF solvent systems were used to prepare the dye solution. To our surprise, we found the solvent affected the overall cell performance significantly. When a dye solution of THF/acetonitrile (THF/AN, v/v = 2/1) was used, it was observed that the V_{OC} values of devices B (zzx-op1−2) and C (zzx-op1−3) were very similar to each other (~102 mV); both were higher than that of device A (zzx-op1, 96 mV). However, the short-circuit current density (J_{SC}) of devices varied in the following order:

$$\text{device A } (5.70 \text{ mA cm}^{-2}) < \text{device C } (6.53 \text{ mA cm}^{-2}) < \text{device B } (7.03 \text{ mA cm}^{-2})$$

As a result, device B with zzx-op1−2 dye gave the highest PCE of 0.279%. This is consistent with its remarkably higher IPCE

Scheme 2. Synthesis Route of zzx-op1−2 and zzx-op1−3

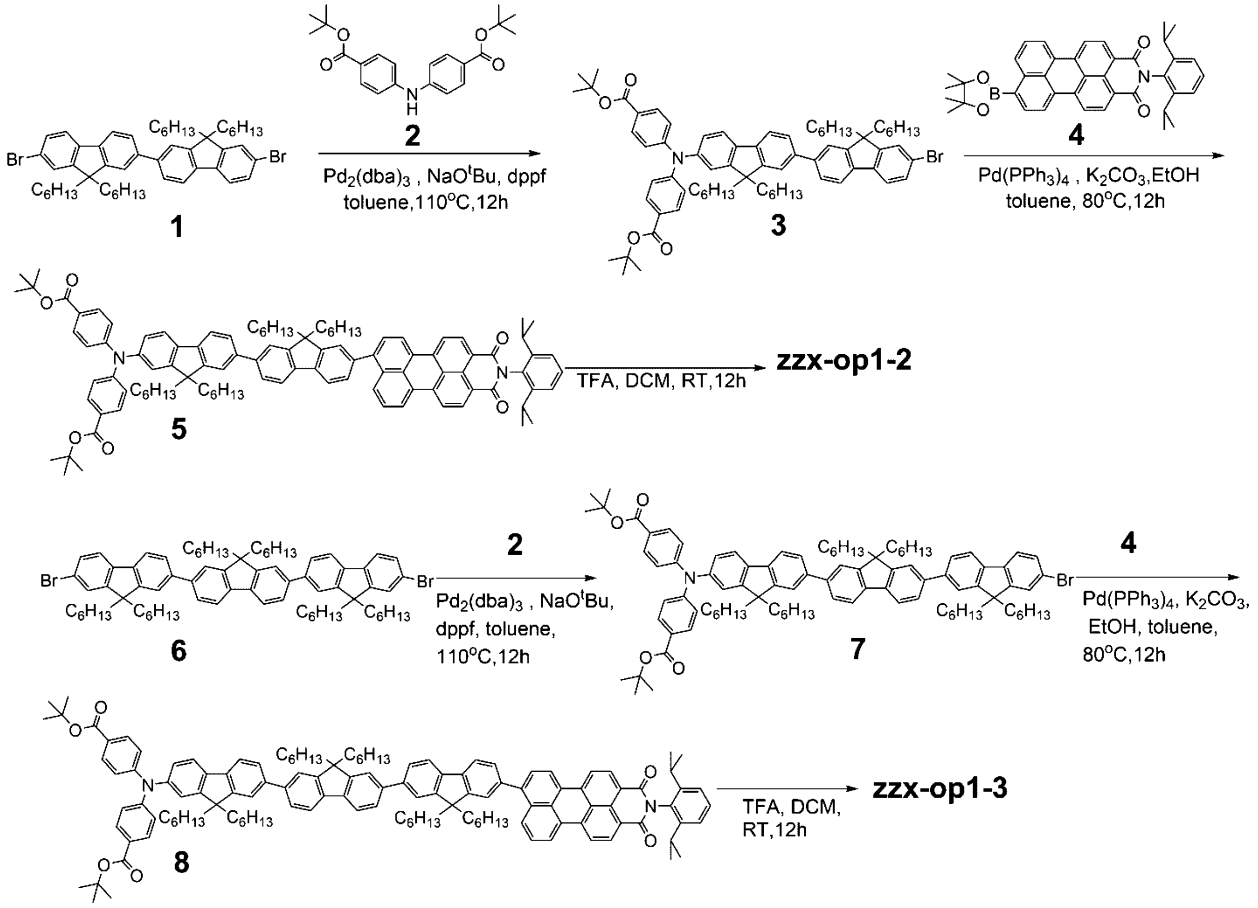

Table 1. Optical and Electrochemical Data of Dyes zzx-op1, zzx-op1−2, and zzx-op1−3

dye	λ_{max} [a] (nm)	E_{ox} [b] (V, vs NHE)	E_{red} [b] (V, vs NHE)	E_{0-0} [c] (eV)	ΔG_{inj} [d] (eV)	ΔG_{reg} [e] (eV)
zzx-op1	354 518	1.28	−0.85	2.21	−0.82	−0.66
zzx-op1−2	362 517	1.24	−0.87	2.23	−0.82	−0.68
zzx-op1−3	369 517	1.24	−0.86	2.23	−0.83	−0.67

[a]Optical properties of all dyes were measured in THF at room temperature. [b]Electrochemical properties of all dyes are measured in THF at room temperature. The supporting electrolyte was 0.1 M $TBAPF_6$. Potentials measured vs ferrocene/ferrocenium (Fc/Fc^+) couple were converted to normal hydrogen electrode (NHE) by addition of +0.63 V. [c]The zero−zero transition energy ($E_{0-0}(S^*)$) was estimated from the intersection of normalized absorption and emission curves. [d]Calculated according to the equation: $\Delta G_{inj} = e[E_{VB}(NiO) - (E_{0-0}(S^*) + E_{red}(S/S^-))]$, $E_{VB}(NiO)$ = 0.54 V vs NHE.[4] [e]Calculated according to the equation: $\Delta G_{reg} = e[E(M/M^-) - E_{red}(S/S^-)]$, $E(I_3^-/I_2^{-\bullet}) = -0.19$ V vs NHE.[33]

with the maximum of 64.3% at 520 nm, compared to the 50.1% for device A with zzx-op1. When dye solutions of THF/AN (v/v = 1.5/1) and THF/AN (v/v = 1/1) were used for zzx-op1−2, both the photocurrent density and open-circuit voltage increased. Device E (with zzx-op1−2 dye) displayed a PCE of 0.353%, a V_{OC} of 117 mV, a fill factor (FF) of 0.40, and a J_{SC} of 7.57 mA cm^{-2}. To the best of our knowledge, this is the highest photocurrent density for *p*-DSSC. Its performance is consistent with the remarkably higher IPCE, with a maximum of 70.2% at 520 nm, as shown in Figure 3.

The increase of photocurrent density in zzx-op1−2 and zzx-op1−3 is consistent with their dye-loading densities on the NiO films. When the zzx-op1−2 was dissolved in THF/AN (v/v = 2/1), THF/AN (v/v = 1.5/1), and THF/AN (v/v = 1/1), the dye-loading density increased from 1.11×10^{-8} mol cm^{-2} μm^{-1}, to 1.24×10^{-8} mol cm^{-2} μm^{-1}, to 1.28×10^{-8} mol cm^{-2} μm^{-1}, because of the augmentation of adsorption−desorption equilibrium constant,[34] the photocurrent density increased from 7.03 mA cm^{-2} to 7.44 mA cm^{-2} to 7.57 mA cm^{-2}. A similar trend was also observed when zzx-op1−3 was dissolved in THF/AN (v/v = 2:1, 0.98×10^{-8} mol cm^{-2} μm^{-1}) and chlorobenzene (1.11×10^{-8} mol cm^{-2} μm^{-1}). However, the discrepancy between dye-loading density and photocurrent density was also observed among three dyes. When the THF/AN (v/v = 2/1) was used as a solvent, the measured dye-loading densities of zzx-op1, zzx-op1−2, and zzx-op1−3 on NiO films were 1.20×10^{-8}, 1.11×10^{-8}, and 0.98×10^{-8} mol cm^{-2} μm^{-1}, respectively. The zzx-op1−2 with a moderate dye-loading density exhibited the highest photocurrent density. When zzx-op1−2 were dissolved in THF/AN (v/v = 2:1) and zzx-op1−3 in chlorobenzene, respectively, an identical dye-loading density (1.11×10^{-8} mol cm^{-2} μm^{-1}) was observed; zzx-op1−2 produced a higher photocurrent density than zzx-op1−3 (7.03 mA cm^{-2} vs 6.68 mA cm^{-2}). This discrepancy indicated the impact of structure difference on the overall cell performance.

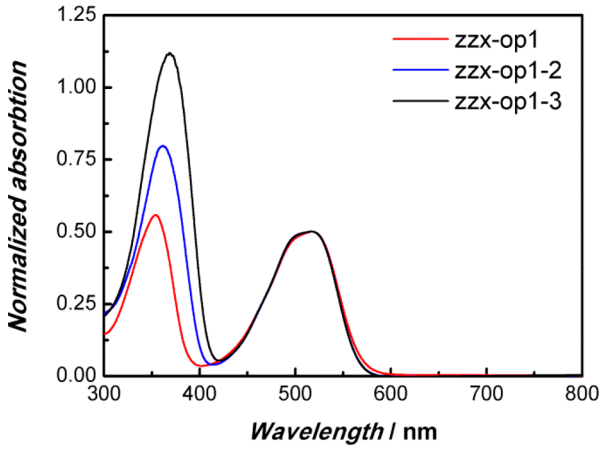

Figure 1. Absorption spectra of zzx-op1, zzx-op1−2, and zzx-op1−3 in THF.

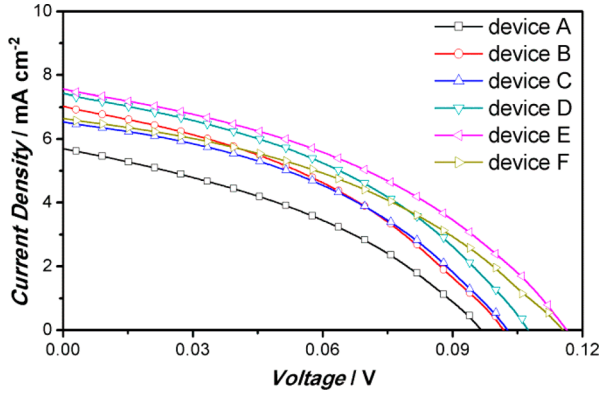

Figure 2. Current−voltage (J−V) characteristics of champion devices under simulated AM 1.5 (100 mW cm^{-2}) conditions. The NiO films for devices A−C were made with dyes zzx-op1, zzx-op1−2, and zzx-op1−3 in THF/AN (v/v = 2/1) solution, devices D and E with zzx-op1−2 in THF/AN (v/v = 1.5/1) and THF/AN (v/v = 1/1), and device F with dye zzx-op1−3 in chlorobenzene.

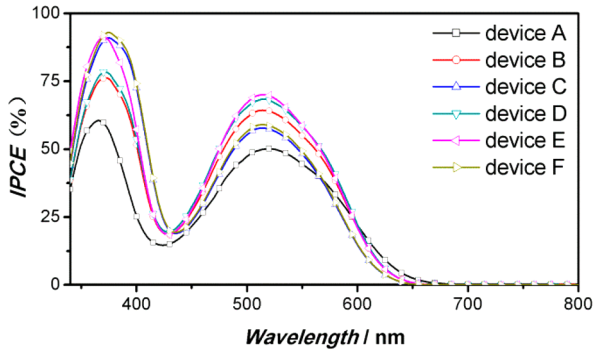

Figure 3. Photocurrent action spectra of devices A−F.

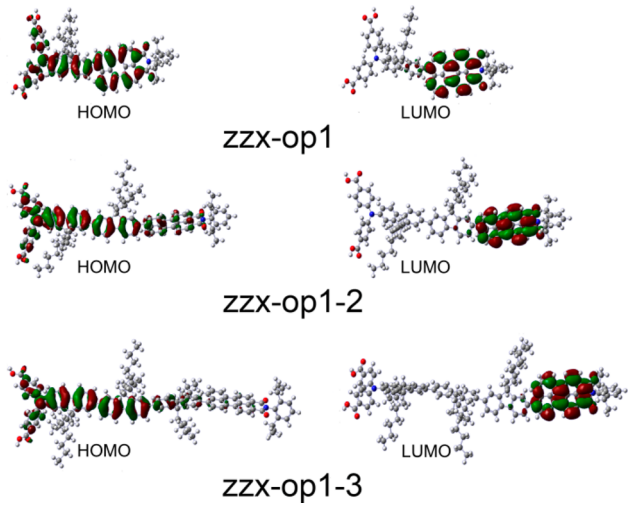

Figure 4. Geometry-optimized structures of zzx-op1, zzx-op1−2, zzx-op1−3 and the electron density distribution of frontier molecular orbitals from DFT calculations with the B3LYP/6-311G(d) model.

The density functional theory (DFT) calculation were performed to study the structural conformation and electron density distribution of the dyes. As shown in Figure 4, the electron density distributions of the lowest unoccupied molecular orbitals (LUMOs) for the three dyes were quite similar to each other and was significantly localized on the PMID unit. The electron density distribution of the highest occupied molecular orbitals (HOMOs) was quite different. In zzx-op1, the electron density in the donor section was more pronounced and was extended significantly to acceptor moiety (PMID unit). In zzx-op1−2, the electron density in the donor reduced with concurrent increase on the first and second FLU unit and extension to PMID unit. In zzx-op1−3, the electron density in the donor reduced with a concurrent increase on the first and second FLU unit and extension to the third FLU unit. In both cases, a disjoint character was observed, which will benefit the charge separation. The length of oligo-fluorene linkers was determined to be 6.90, 18.3, and 26.8 Å for zzx-op1, zzx-op1−2, and zzx-op1−3, respectively. The spatial distribution of the dyes is in an approximately straight line, and thus the molecule might be aligned predominantly perpendicular to the NiO surface. (The detailed torsion angle of π-linkers and PMID are shown in the Table S1 in the ESI.) The dyes with longer linkers (zzx-op1−2 and zzx-op1−3) presented better energy conversion efficiency, which was also observed in several other systems.[7,35]

Table 2. Photovoltaic Data of zzx-op1, zzx-op1−2, and zzx-op1−3 Sensitized Champion Solar Cells under an Illumination of 100 mW cm^{-2}, AM1.5G Conditions

device	dye	solvent (v/v)	J_{SC} (mA cm^{-2})	V_{OC} (V)	fill factor, ff	η (%)
A	zzx-op1	THF/AN (2/1)	5.70	96	0.38	0.207
B	zzx-op1−2	THF/AN (2/1)	7.03	102	0.39	0.279
C	zzx-op1−3	THF/AN (2/1)	6.53	103	0.41	0.276
D	zzx-op1−2	THF/AN (1.5/1)	7.44	106	0.41	0.322
E	zzx-op1−2	THF/AN (1/1)	7.57	117	0.40	0.353
F	zzx-op1−3	chlorobenzene	6.68	115	0.40	0.308

dx.doi.org/10.1021/am5022396 | ACS Appl. Mater. Interfaces 2014, 6, 10614−10622

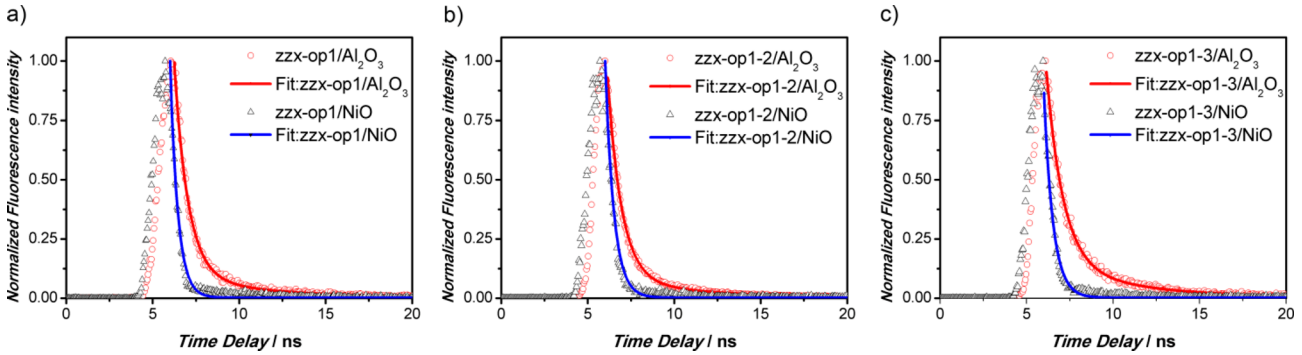

Figure 5. Time-resolved PL decay traces of dye-sensitized NiO films (black triangle, △), Al_2O_3 films (red circle, ○), fitted line for dyes on NiO film (blue line), Al_2O_3 film (red lines): (a) zzx-op1, (b) zzx-op1−2, and (c) zzx-op1−3. Excitation wavelength = 445 nm.

Time-resolved fluorescence decays measurements were performed to evaluate the hole injection kinetics. The measurements were performed on dye-coated NiO films and compared with those from Al_2O_3 films.[36−39] The NiO films and Al_2O_3 films with the same thickness ($L \approx 3.0$ μm) were used. The result is shown in Figure. 5. To resolve the hole injection kinetics, the time coefficients from an amplitude-averaged decay time model were used to determine the corresponding rate coefficients, $k_{NiO} = \tau_{NiO}^{-1}$ and $k_{Al_2O_3} = \tau_{Al_2O_3}^{-1}$, according to the report of Diau et al.[36,40] In this model, the decay data were fitted with a parallel kinetic model:

$$A \rightarrow B,\ \tau_1$$

$$A' \rightarrow B',\ \tau_2$$

$$f(t) = a\exp\left(-\frac{t}{\tau_1}\right) + b\exp\left(-\frac{t}{\tau_2}\right)$$

Components A and A′ are described with a single-exponential function and decay coefficients τ_1 and τ_2, respectively. The pre-exponential factors a and b represent the relative weights (or amplitudes) of components A and A′, respectively. For Al_2O_3 films, two decay components are required to fit the fluorescence transients. This is because the PL decays of the dye-coated Al_2O_3 films reflect the radiative decay to the ground state, as well as intermolecular energy transfer, because of aggregation of the dye on the surface of Al_2O_3 film. These two processes were in the similar time scale. For NiO films, only one component is required to fit the data. This is because the hole injection is much faster than intermolecular energy transfer (IET). Because of the limitation of our instrumentation, the observed decay profiles only reflected the IET, which was of course affected by hole injection into the valence band of NiO.[36] Assuming the dye aggregation on the NiO and Al_2O_3 was similar when the absorption of the films are same, and the nonradiative relaxations are also similar to each other, the averaged fluorescence lifetime therefore can be used to reveal the hole injection kinetics. The average fluorescence lifetimes for zzx-op1, zzx-op1−2, and zzx-op1−3 sensitized Al_2O_3 films were evaluated to be 2.27, 2.26, 2.70 ns, respectively, while the strong quenching of the emission for those dyes were observed when they were stained on the NiO films. Considering the reconvolution of the instrument response function of ∼89 ps, the IRF response and the data fitting results with parallel kinetics model indicated that the lifetime of the emission of the three dyes stained on the NiO films were 0.44, 0.50, and 0.53 ns, respectively. This result confirms a rapid hole injection from the excited state of the dye into the valence band of NiO.[37] The hole injection quantum yield can be approximately described according to the equation $\Phi_{inj} = 1 - \tau_{NiO}/\tau_{Al_2O_3}$, which was 80% (zzx-op1), 78% (zzx-op1−2), and 80% (zzx-op1−3), respectively.[36] It indicates that the three dyes showed nearly identical hole injection process. It should be mentioned that the injection yield could be higher than those showed here due to deadsorbed dye inside the films.

The dark current and electrochemical impedance spectroscopy (EIS) studies revealed different charge recombination behavior of devices from three dyes.[5,22,41−43] As shown in Figure 6, the zzx-op1 and zzx-op1−2 sensitized cells (devices A and B) exhibited smaller dark current densities than that of zzx-op1−3 sensitized cell (device C) at the same bias, implying compact layers of zzx-op1 and zzx-op1−2 on the surface of the NiO particles were formed to prevent the charge recombination between the injected hole and the hole acceptor in electrolytes. This is consistent with higher recombination resistance observed for devices A and B in impedance results. When different solvent systems were used, smaller dark current densities were observed for devices D and E. In EIS study, the NiO/dye/electrolyte interfacial charge transfer resistance (i.e., charge recombination resistance, R_{rec}) was evaluated using a transmission line model.[42−44] As shown in Figure 7, device A (zzx-op1) and device B (zzx-op1−2) showed higher R_{rec} than device C (zzx-op1−3) at a given bias. This result agrees with the observation on the dark current, indicating device C

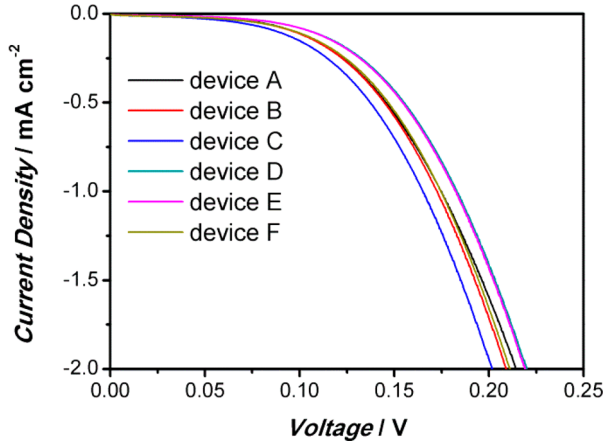

Figure 6. Dark current density as a function of applied bias obtained from dark current measurement of devices A−F.

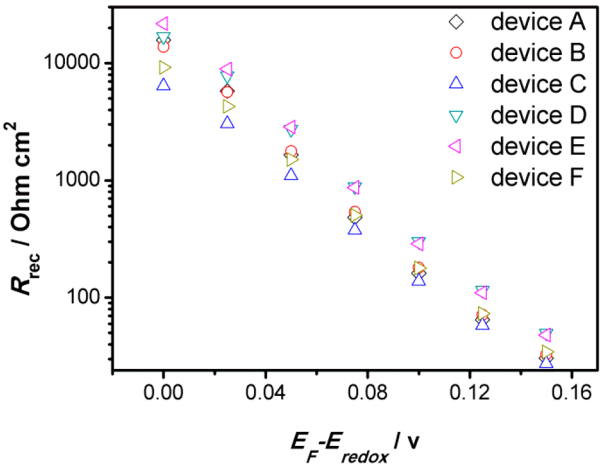

Figure 7. Interfacial charge recombination resistance (R_{rec}), as a function of applied bias obtained from electrochemical impedance measurement in darkness for devices A–F.

suffered from charge recombination between the injected hole and hole acceptor in electrolytes. This implies that zzx-op1 and zzx-op1–2 might form a more compact dye layers on the surface of NiO films than zzx-op1–3 when THF/AN (v/v = 2/1) was used. The situation can be changed with the solvent. For example, device F exhibited an increased R_{rec} value, which was due to the application of chlorobenzene.

Transient photovoltage/photocurrent decay measurements showed longer hole lifetime in zzx-op1–2 sensitized solar cells.[45,46] Figure 8a presents plots of the hole density as a

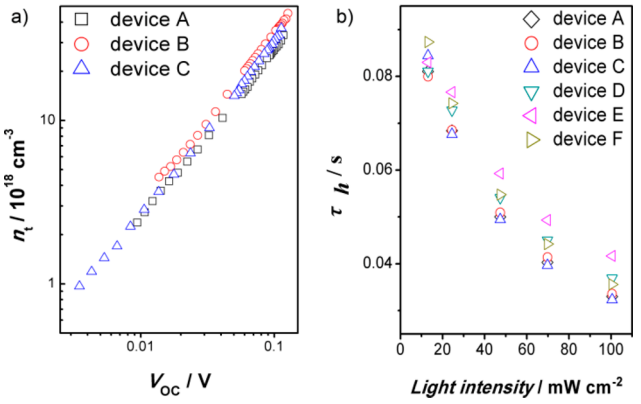

Figure 8. Transient photovoltage/photocurrent decay and charge-extraction measurements: (a) hole density as a function of bias voltage (V_{OC}) of devices A, B, and C; (b) hole lifetime as a function of light intensity of devices A–F.

function of the potential bias of device A (zzx-op1), device B (zzx-op1–2), and device C (zzx-op1–3). It perceived that devices B and C exhibited higher hole density than that of device A. As illustrated in Figure 8b, under the same light intensity, device B exhibited longer hole lifetime (τ_h) than that of devices A and C. These results are quite fitted with the results from dark current and impedance measurements. In the case of zzx-op1–2, as illustrated in Figure 8b, device E exhibited a longer lifetime than that of device B under the same light intensity. This was attributed to a more compact dye block layer for device E, efficiently retarding the charge recombination between the injected holes and the hole acceptor in electrolytes.

In *p*-DSSC, the overall performance linked tightly to the charge recombination of the injected hole in a semiconductor with the reduced dye (process A) and with hole acceptor in electrolyte (process B), as shown in Figure 9.[4,5] It is critical to

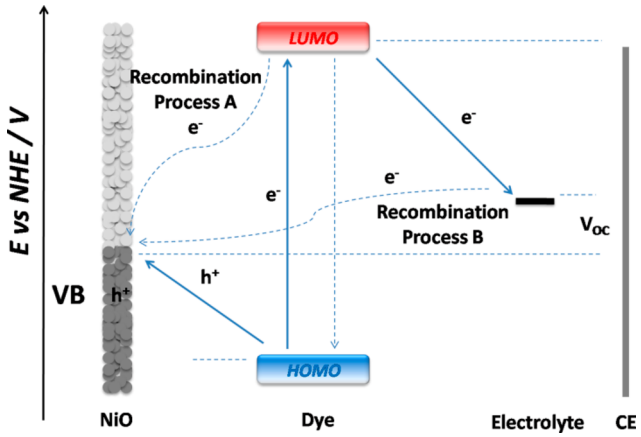

Figure 9. Schematic of charge transfer process in *p*-DSSC, arrows with solid lines denote desired transfer for energy conversion, and those with dashed lines denote undesired transfer. Recombination Process A represents the recombination between the injected hole and the reduced dye, and Recombination Process B represents the recombination between the injected hole in NiO film and the hole acceptor in electrolyte.

reduce such recombination in order to obtain better performance. This could be achieved by either applying a thin layer of metal oxide, depositing an insulation layer, or forming a more compact layer of organic dyes, providing a shield layer for the charge recombination.[47–52] This can be used to explain the different photovoltaic performance of zzx-op1, zzx-op1–2, and zzx-op1–3. As illustrated in Figure 10, when the dyes adsorbed

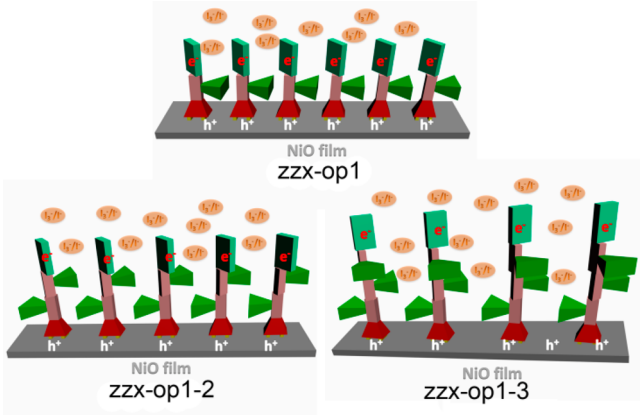

Figure 10. Pictorial representation of the self-assembled dye layer of zzx-op1, zzx-op1–2, and zzx-op1–3 on the surface of NiO.

on the NiO nanoparticles, they tend to anchored vertically on the surface of NiO nanoparticles due to the "Y"-shaped feature.[7] The zzx-op1 with a more rigid structure formed a much compact dye layer, which retarded Recombination Process B. However, it will not provide sufficient shielding to retard Recombination Process A, because of the short length between the PMID unit and the surface of NiO nanoparticles.

dx.doi.org/10.1021/am5022396 | ACS Appl. Mater. Interfaces 2014, 6, 10614–10622

The zzx-op1−3, having the longest molecule length, effectively retarded Recombination Process A,[7] but not Recombination Process B. The less-compacted dye layer on the surface of NiO nanoparticles provides a large void for easy penetration of iodide electrolyte into dye assembly to increase the recombination probability of process B. The dye zzx-op1−2 with moderate length formed a compact dye layer, which could retard Recombination Processes A and B simultaneously. As a result, the dye zzx-op1−2 achieved better device performance than zzx-op1 and zzx-op1−3.

Finally, the long-term stability zzx-op1−2 sensitized solar cell (device E) was evaluated in darkness. Figure S7 in the Supporting Information shows the evolution of photovoltaic parameters of device E stored in darkness at ambient temperature (20 °C). During a month-long period of time, only a slight decrease of J_{SC} and V_{OC} was observed. Meanwhile, an averaged photocurrent density of 7.27 mA cm^{-2} was observed. The PCE remained almost unchanged, with a slightly increased fill factor. This impressive result is indicative of the superior thermal stability of *p*-DSSC devices based on oligo-fluorene-based organic dyes.

CONCLUSIONS

In summary, we have synthesized three oligo-fluorene-based organic push−pull dyes for *p*-DSSC. The unprecedented photocurrent density of 7.57 mA cm^{-2} with a power conversion efficiency (PCE) of 0.357% was achieved under AM 1.5G conditions. Time-resolved fluorescence decays measurement showed that three dyes were energetically favorable for efficient hole injection. The dark current and electrochemical impedance measurements revealed that the zzx-op1 and zzx-op1−2 sensitized cells (devices A and B) exhibited smaller dark current densities than that of the zzx-op1−3 sensitized cell. Transient photovoltage/photocurrent decay measurements showed longer electron lifetime in zzx-op1−2 sensitized solar cells. All results indicated that the dye zzx-op1−2 formed a much more compact dye block layer than zzx-op1 and zzx-op1−3, with regard to retarding the charge recombination between the injected hole in the NiO film and the hole acceptor in the electrolyte. The long-term stability study also showed the superior stability of *p*-DSSC devices based on oligo-fluorene-based organic dye.

EXPERIMENTAL SECTION

Devices Fabrication. NiO nanoparticle powder from Inframat (72.2 wt % Ni, Catalog No. 28N-0801, particle size ≈ 20 nm, BET multipoint specific surface area, SSA > 50 m^2/g) was used as received. NiO paste was prepared by mixing an ethyl cellulose solution in ethanol (44 wt %), terpineol (46 wt %), and NiO (10 wt %). The paste was screen-printed on FTO glass (NSG 15Ω/□, 2.2 mm thick) by a commercial semiautomatic screen printer. The films were dried for 10 min at 120 °C. The thickness of films (3.1 μm thick) was determined by a profile system (DEKTAK, VEECCO, Bruker). The films were then sintered under an air flow at 500 °C for 30 min with a ramping time of 40 min from room temperature (~25 °C) to 500 °C and then cooled to 80 °C in air. The films were then dipped into a dye solution either in a mixture of THF/AN or chlorobenzene at room temperature for 18 h. After washing with acetonitrile and drying with air flow, the sensitized NiO working electrode and the counter electrode were assembled together using a 25-μm-thick Surlyn gasket. A pneumatic finger press was used to press the working electrode while heating the counter electrode. The counter electrodes were produced by applying one drop of H_2PtCl_6 (10 mM in ethanol) to FTO glass and thermally decomposing by firing at 400 °C for 15 min under a gentle flow of air. The electrolyte (1.0 M LiI, 0.1 M I_2 in acetonitrile) was vacuum-backfilled in the cell cavity. The backfilled hole was sealed using an aluminum-Surlyn sheet, which was prepared by heating aluminum foil with a 25-μm Surlyn sheet on a hot plate at 120 °C.

Devices Characterization. A 450 W xenon light source solar simulator (Oriel, model 9119) with an AM 1.5G filter (Oriel, model 91192) was used to give an irradiance of 100 mW cm^{-2} at the surface of the solar cells. The current voltage characteristics of the devices under these conditions were obtained by applying external potential bias to the devices and measuring the generated photocurrent with a digital sourcemeter (Keithley, Model 2400, USA). A similar data acquisition system was used to control the incident photon-to-current conversion efficiency (IPCE) measurement. A white light bias (1% sunlight intensity) was applied onto the devices during the IPCE measurements with the AC model (10 Hz). The devices with the photoanode area of 0.40 cm × 0.40 cm were tested with a metal mask: 0.30 cm × 0.30 cm to prevent the scattering light.

ASSOCIATED CONTENT

Supporting Information

Synthetic procedures and characterization data of all new compounds, emission spectra, absorption spectra on NiO nanoparticles, cyclic voltammogram, PL decay, EIS and long-term stability data. This material is available free of charge via the Internet at http://pubs.acs.org.

AUTHOR INFORMATION

Corresponding Authors

*E-mail: zhixin-zhao@hust.edu.cn (Z. Zhao).
*E-mail: mingkui.wang@mail.hust.edu.cn (M. Wang).
*E-mail: hhe@eiu.edu (H. He).

Author Contributions

The manuscript was written through contributions of all authors. All authors have given approval to the final version of the manuscript.

Notes

The authors declare no competing financial interest.

ACKNOWLEDGMENTS

This work was partially supported by the National Basic Research Program of China (973 program, Grant No. 2011CBA00703), the Fundamental Research Funds for the Central Universities (Grant No. HUST: 2014TS016, to Z. Zhao), and Council on Faculty Research, Eastern Illinois University (to H. He). Q.A. acknowledges a Swinburne University Postgraduate Research Award (SUPRA) and F.W. thanks the National Computational Infrastructure (NCI) at the Australian National University, under the Merit Allocation Scheme (MAS) and Swinburne University Supercomputing Facilities (Green/gSTAR) for computer resources.

REFERENCES

(1) O'Regan, B.; Grätzel, M. A Low-Cost, High-Efficiency Solar Cell Based on Dye-Sensitized Colloidal TiO_2 Films. *Nature* **1991**, 737−740.
(2) Grätzel, M. Recent Advances in Sensitized Mesoscopic Solar Cells. *Acc. Chem. Res.* **2009**, *42*, 1788−1798.
(3) Hagfeldt, A.; Boschloo, G.; Sun, L.; Kloo, L.; Pettersson, H. Dye-Sensitized Solar Cells. *Chem. Rev.* **2010**, *110*, 6595−6663.
(4) Odobel, F.; Le Pleux, L.; Pellegrin, Y.; Blart, E. New Photovoltaic Devices Based on the Sensitization of *p*-type Semiconductors: Challenges and Opportunities. *Acc. Chem. Res.* **2010**, *43*, 1063−1071.
(5) Odobel, F.; Pellegrin, Y.; Gibson, E. A.; Hagfeldt, A.; Smeigh, A. L.; Hammarström, L. Recent Advances and Future Directions to

Optimize the Performances of *p*-Type Dye-Sensitized Solar Cells. *Coord. Chem. Rev.* **2012**, *256*, 2414−2423.
(6) Yamada, K.; Fukuda, R.; Yamamoto, K.; Sonoda, T.; Nakamura, H.; Yamane, H. Effect of *p*-Type Semiconductor Electrode on Photovoltaic Properties in *n*/*p* Tandem-Type Dye-Sensitized Solar Cell. *Mol. Cryst. Liq. Cryst.* **2012**, *566*, 193−201.
(7) Nattestad, A.; Mozer, A. J.; Fischer, M. K. R.; Cheng, Y. B.; Mishra, A.; Bäuerle, P.; Bach, U. Highly Efficient Photocathodes For Dye-Sensitized Tandem Solar Cells. *Nat. Mater.* **2010**, *9*, 31−35.
(8) Odobel, F.; Pellegrin, Y. Recent Advances in the Sensitization of Wide-Band-Gap Nanostructured *p*-Type Semiconductors. Photovoltaic and Photocatalytic Applications. *J. Phys. Chem. Lett.* **2013**, *1*, 2551−2564.
(9) Powar, S.; Wu, Q.; Weidelener, M.; Nattestad, A.; Hu, Z.; Mishra, A.; Bäuerle, P.; Spiccia, L.; Cheng, Y.; Bach, U. Improved Photocurrents for p-Type Dye-Sensitized Solar Cells Using Nanostructured Nickel(II) Oxide Microballs. *Energy Environ. Sci.* **2012**, *5*, 8896−8900.
(10) Yella, A.; Lee, H.; Hoi Nok Tsao, C. Y.; Chandiran, A. K.; Nazeeruddin, M. K.; Diau, E. W.; Yeh, C.; Zakeeruddin, S. M.; Grätzel, M. Porphyrin-Sensitized Solar Cells with Cobalt(II/III)-Based Redox Electrolyte Exceed 12 Percent Efficiency. *Science* **2011**, *334*, 629−634.
(11) Li, L.; Diau, E. W. Porphyrin-Sensitized Solar Cells. *Chem. Soc. Rev.* **2013**, *42*, 291−304.
(12) O'Regan, B. C.; Durrant, J. R. Kinetic and Energetic Paradigms for Dye-Sensitized Solar Cells: Moving from the Ideal to the Real. *Acc. Chem. Res.* **2009**, *42*, 1799−1808.
(13) Mathew, S.; Yella, A.; Gao, P.; Humphry-Baker, R.; Curchod, B. F. E.; Ashari-Astani, N.; Tavernelli, I.; Rothlisberger, U.; Nazeeruddin, M. K.; Grätzel, M. Dye-Sensitized Solar Cells with 13% Efficiency Achieved through the Molecular Engineering of Porphyrin Sensitizers. *Nat. Chem.* **2014**, *6*, 242−247.
(14) Powar, S.; Daeneke, T.; Ma, M. T.; Dongchuan, F.; Duffy, N. W.; Götz, G.; Weidelener, M.; Mishra, A.; Bäuerle, P.; Spiccia, L.; Bach, U. Highly Efficient *p*-Type Dye-Sensitized Solar Cells based on Tris(1,2-diaminoethane)Cobalt(II)/(III) Electrolytes. *Angew. Chem., Int. Ed.* **2013**, *52*, 602−605.
(15) Morandeira, A.; Boschloo, G.; Hagfeldt, A.; Hammarström, L. Photoinduced Ultrafast Dynamics of Coumarin 343 Sensitized *p*-Type-Nanostructured NiO Films. *J. Phys. Chem. B* **2005**, *109*, 19403−19410.
(16) Borgström, M.; Blart, E.; Boschloo, G.; Mukhtar, E.; Hagfeldt, A.; Hammarström, L.; Odobel, F. Sensitized Hole Injection of Phosphorus Porphyrin into NiO: Toward New Photovoltaic Devices. *J. Phys. Chem. B* **2005**, *109*, 22928−22934.
(17) Morandeira, A.; Fortage, J.; Edvinsson, T.; Le Pleux, L.; Blart, E.; Boschloo, G.; Hagfeldt, A.; Hammarström, L.; Odobel, F. Improved Photon-to-Current Conversion Efficiency with a Nanoporous *p*-Type NiO Electrode by the Use of a Sensitizer-Acceptor Dyad. *J. Phys. Chem. C* **2008**, *112*, 1721−1728.
(18) Mori, S.; Fukuda, S.; Sumikura, S.; Takeda, Y.; Tamaki, Y.; Suzuki, E.; Abe, T. Charge-Transfer Processes in Dye-Sensitized NiO Solar Cells. *J. Phys. Chem. C* **2008**, *112*, 16134−16139.
(19) Qin, P.; Zhu, H.; Edvinsson, T.; Boschloo, G.; Hagfeldt, A.; Sun, L. Design of an Organic Chromophore for *p*-Type Dye-Sensitized Solar Cells. *J. Am. Chem. Soc.* **2008**, *130*, 8570−8571.
(20) Le Pleux, L.; Smeigh, A. L.; Gibson, E.; Pellegrin, Y.; Blart, E.; Boschloo, G.; Hagfeldt, A.; Hammarström, L.; Odobel, F. Synthesis, Photophysical and Photovoltaic Investigations of Acceptor-Functionalized Perylene Monoimide Dyes for Nickel Oxide *p*-Type Dye-Sensitized Solar Cells. *Energy Environ. Sci.* **2011**, *4*, 2075−2084.
(21) Qin, P.; Wiberg, J.; Gibson, E. A.; Linder, M.; Li, L.; Brinck, T.; Hagfeldt, A.; Albinsson, B.; Sun, L. Synthesis and Mechanistic Studies of Organic Chromophores with Different Energy Levels for *p*-Type Dye-Sensitized Solar Cells. *J. Phys. Chem. C* **2010**, *114*, 4738−4748.
(22) Weidelener, M.; Mishra, A.; Nattestad, A.; Powar, S.; Mozer, A. J.; Mena-Osteritz, E.; Cheng, Y.; Bach, U.; Bäuerle, P. Synthesis and Characterization of Perylene−Bithiophene−Triphenylamine Triads: Studies on the Effect of Alkyl-Substitution in *p*-Type NiO based Photocathodes. *J. Mater. Chem.* **2012**, *22*, 7366−7379.
(23) Yen, Y.; Chen, W.; Hsu, C.; Chou, H.; Lin, J. T.; Yeh, M. P. Arylamine-Based Dyes for *p*-Type Dye-Sensitized Solar Cells. *Org. Lett.* **2011**, *13*, 4930−4933.
(24) Chang, C.; Chen, Y.; Hsu, C.; Chou, H.; Lin, J. T. Squaraine-Arylamine Sensitizers for Highly Efficient *p*-Type Dye-Sensitized Solar Cells. *Org. Lett.* **2012**, *14*, 4726−4729.
(25) Ji, Z.; Natu, G.; Huanga, Z.; Wu, Y. Linker Effect in Organic Donor-Acceptor Dyes for *p*-Type NiO Dye Sensitized Solar Cells. *Energy Environ. Sci.* **2011**, *4*, 2818−2821.
(26) Favereau, L.; Warnan, J.; Pellegrin, Y.; Blart, E.; Boujtita, M.; Jacquemin, D.; Odobel, F. Diketopyrrolopyrrole Derivatives for Efficient NiO-Based Dye-Sensitized Solar Cells. *Chem. Commun.* **2013**, *49*, 8018−8020.
(27) Warnan, J.; Gardner, J.; Pleux, L. L.; Petersson, J.; Pellegrin, Y.; Blart, E.; Hammarström, L.; Odobel, F. Multichromophoric Sensitizers Based on Squaraine for NiO Based Dye-Sensitized Solar Cells. *J. Phys. Chem. C* **2014**, *118*, 103−113.
(28) Li, L.; Gibson, E. A.; Qin, P.; Boschloo, G.; Gorlov, M.; Hagfeldt, A.; Sun, L. Double-Layered NiO Photocathodes for *p*-Type DSSCs with Record IPCE. *Adv. Mater.* **2010**, *22*, 1759−1762.
(29) Liu, Z.; Xiong, D.; Xu, X.; Arooj, Q.; Wang, H.; Yin, L.; Li, W.; Wu, H.; Zhao, Z.; Chen, W.; Wang, M.; Wang, F.; Cheng, Y.; He, H. Modulated Charge Injection in *p*-Type Dye-Sensitized Solar Cells Using Fluorene-based Light Absorbers. *ACS Appl. Mater. Interfaces* **2014**, *6*, 3448−3454.
(30) Jo, J.; Chi, C.; Höger, S.; Wegner, G.; Yoon, D. Y. Synthesis and Characterization of Monodisperse Oligofluorenes. *Chem.—Eur. J.* **2004**, *10*, 2681−2688.
(31) P. Aldred, M.; Li, C.; Zhang, G.; Gong, W.; Li, A. D. Q.; Dai, Y.; Ma, D.; Zhu, M. Fluorescence Quenching and Enhancement of Vitrifiable Oligofluorenes End-Capped with Tetraphenylethene. *J. Mater. Chem.* **2012**, *22*, 7515−7528.
(32) Cui, Y.; Wu, Y.; Lu, X.; Zhang, X.; Zhou, G.; Miapeh, F. B.; Zhu, W.; Wang, Z. Incorporating Benzotriazole Moiety to Construct D-A-π-A Organic Sensitizers for Solar Cells: Significant Enhancement of Open-Circuit Photovoltage with Long Alkyl Group. *Chem. Mater.* **2011**, *23*, 4394−4401.
(33) Gibson, E. A.; Le Pleux, L.; Fortage, J.; Pellegrin, Y.; Blart, E.; Odobel, F.; Hagfeldt, A.; Boschloo, G. Role of the Triiodide/Iodide Redox Couple in Dye Regeneration in *p*-Type Dye-Sensitized Solar Cells. *Langmuir* **2012**, *28*, 6485−6493.
(34) Cai, N.; Li, R.; Wang, Y.; Zhang, M.; Wang, P. Organic Dye-Sensitized Solar Cells with a Cobalt Redox Couple: Influences of π-Linker Rigidification and Dye-Bath Solvent Selection. *Energy Environ. Sci.* **2013**, *6*, 139−147.
(35) Zhu, L.; Yang, H. B.; Zhong, C.; Li, C. M. Rational Design of Triphenylamine Dyes for Highly Efficient *p*-Type Dye Sensitized Solar Cells. *Dyes Pigm.* **2014**, *105*, 97−104.
(36) Lu, H.; Tsai, C.; Yen, W.; Hsieh, C.; Lee, C.; Yeh, C.; Diau, E. W. Control of Dye Aggregation and Electron Injection for Highly Efficient Porphyrin Sensitizers Adsorbed on Semiconductor Films with Varying Ratios of Coadsorbate. *J. Phys. Chem. C* **2009**, *113*, 20990−20997.
(37) Chang, Y.; Wu, H.; Reddy, N. M.; Lee, H.; Lu, H.; Yeh, C.; Diau, E. W. The Influence of Electron Injection and Charge Recombination Kinetics on the Performance of Porphyrin-Sensitized Solar Cells: Effects of the 4-*tert*-butylpyridine Additive. *Phys. Chem. Chem. Phys.* **2013**, *15*, 4651−4655.
(38) Wu, X.; Xing, G.; Tan, S. L. J.; Webster, R. D.; Sum, T. C.; Yeow, E. K. L. Hole Transfer Dynamics from Dye Molecules to *p*-Type NiO Nanoparticles: Effects of Processing Conditions. *Phys. Chem. Chem. Phys.* **2012**, *14*, 9511−9519.
(39) Koops, S. E.; O Regan, B. C.; Barnes, P. R. F.; Durrant, J. R. Parameters Influencing the Efficiency of Electron Injection in Dye-Sensitized Solar Cells. *J. Am. Chem. Soc.* **2009**, *131*, 4808−4818.
(40) Luo, L.; Lo, C.; Lin, C.; Chang, I.; Diau, E. W. Femtosecond Fluorescence Dynamics of Porphyrin in Solution and Solid Films: The

Effects of Aggregation and Interfacial Electron Transfer between Porphyrin and TiO_2. *J. Phys. Chem. B* **2006**, *110*, 410−419.
(41) Huang, Z.; Natu, G.; Ji, Z.; Hasin, P.; Wu, Y. Electrochemical Impedance Spectroscopic Analysis of Dye-Sensitized Solar Cells. *J. Phys. Chem. C* **2011**, *115*, 25109−25114.
(42) Wang, Q.; Moser, J.; Grätzel, M. *p*-Type Dye-Sensitized NiO Solar Cells: A Study by Electrochemical Impedance Spectroscopy. *J. Phys. Chem. B* **2005**, *109*, 14945−14953.
(43) Wang, M.; Chen, P.; Humphry-Baker, R.; Zakeeruddin, S. M.; Grätzel, M. The Influence of Charge Transport and Recombination on the Performance of Dye-Sensitized Solar Cells. *ChemPhysChem* **2009**, *10*, 290−299.
(44) Zhu, L.; Yang, H.; Zhong, C.; Li, C. M. Modified Triphenylamine-Dicyanovinyl-Based Donor-Acceptor Dyes with Enhanced Power Conversion Efficiency of *p*-Type Dye-Sensitized Solar Cells. *Chem.—Asian J.* **2012**, *7*, 2791−2795.
(45) Bisquert, J.; Zaban, A.; Greenshtein, M.; Mora-Seró, I. Determination of Rate Constants for Charge Transfer and the Distribution of Semiconductor and Electrolyte Electronic Energy Levels in Dye-Sensitized Solar Cells by Open-Circuit Photovoltage Decay Method. *J. Am. Chem. Soc.* **2004**, *126*, 13550−13559.
(46) Bai, J.; Xu, X.; Xu, L.; Cui, J.; Huang, D.; Chen, W.; Cheng, Y.; Shen, Y.; Wang, M. Potassium-Doped Zinc Oxide as Photocathode Material in Dye-Sensitized Solar Cells. *ChemSusChem* **2013**, *6*, 622−629.
(47) Koumura, N.; Wang, Z.; Mori, S.; Miyashita, M.; Suzuki, E.; Hara, K. Alkyl-Functionalized Organic Dyes for Efficient Molecular Photovoltaics. *J. Am. Chem. Soc.* **2006**, *128*, 14256−14257.
(48) Nelson, J.; Chandler, R. E. Random Walk Models of Charge Transfer and Transport in Dye Sensitized Systems. *Coord. Chem. Rev.* **2004**, *248*, 1181−1194.
(49) Katoh, R.; Furube, A.; V. Barzykin, A.; Arakawa, H.; Tachiya, M. Kinetics and Mechanism of Electron Injection and Charge Recombination in Dye-Sensitized Nanocrystalline Semiconductors. *Coord. Chem. Rev.* **2004**, *248*, 1195−1213.
(50) Natu, G.; Huang, Z.; Ji, Z.; Wu, Y. The Effect of an Atomically Deposited Layer of Alumina on NiO in *p*-Type Dye-Sensitized Solar Cells. *Langmuir* **2012**, *28*, 950−956.
(51) Wang, M.; Liu, J.; Cevey-Ha, N.; Moon, S.; Liska, P.; Humphry-Baker, R.; Moser, J.; Grätzel, C.; Wang, P.; Zakeeruddin, S. M.; Grätzel, M. High Efficiency Solid-state Sensitized Heterojunction Photovoltaic Device. *Nano Today* **2010**, *5*, 169−174.
(52) Kuang, D.; Ito, S.; Wenger, B.; Klein, C.; Moser, J.; Humphry-Baker, R.; Zakeeruddin, S. M.; Grätzel, M. High Molar Extinction Coefficient Heteroleptic Ruthenium Complexes for Thin Film Dye-Sensitized Solar Cells. *J. Am. Chem. Soc.* **2006**, *128*, 4146−4154.